JGR Biogeosciences

RESEARCH ARTICLE
10.1029/2023JG007435

Assessing the Deep Carbon Release in an Active Volcanic Field Using Hydrochemistry, $\delta^{13}C_{DIC}$ and $\Delta^{14}C_{DIC}$

Jun Zhong[1], Linan Wang[1], Antonio Caracausi[2,3], Albert Galy[4], Si-Liang Li[1], Wanfa Wang[5], Maoliang Zhang[1], Cong-Qiang Liu[1], Guo-Ming Liu[6], and Sheng Xu[1]

[1]Institute of Surface-Earth System Science, School of Earth System Science, Tianjin University, Tianjin, China, [2]Istituto Nazionale di Geofisica e Vulcanologia – Sezione di Palermo, Palermo, Italy, [3]Departamento de Geología, Universidad de Salamanca, Salamanca, Spain, [4]UL-CNRS-CRPG, Vandœuvre-l`es-Nancy, France, [5]College of Resources and Environmental Engineering, Key Laboratory of Karst Georesources and Environment, Ministry of Education, Guizhou University, Guiyang, China, [6]Changbaishan Tianchi Volcano Observatory, Antu, China

Abstract Volcanic activities have great implications on the geological carbon cycle, and ascertaining the deep carbon contribution in the Earth's surface that runs along the volcanic edifices is important to understand the relationship between solid Earth degassing and global climate change. This study reports analytical results of major dissolved ions concentrations, carbon isotopic compositions ($\delta^{13}C_{DIC}$ and $\Delta^{14}C_{DIC}$) of dissolved inorganic carbon (DIC) of rivers, cold springs, and hot springs from Changbaishan volcanic area, Northeast China. The hydrothermal fluids had a significant impact on solutes budgets, as well as carbon isotopes for the rivers. The changes in concentrations of major ions are mainly controlled by mixing of high-temperature water/rock interaction and low-temperature water/rock interaction, and low-temperature water/rock interaction can be explained by the change of chemical composition between volcanic cone (trachyte) and basaltic shield. Because $\Delta^{14}C_{DIC}$ is conservative to CO_2 outgassing, we used $\Delta^{14}C_{DIC}$ to figure out the contributions of deep carbon and surface carbon. While $\delta^{13}C_{DIC}$ is sensitive to CO_2 outgassing, we thus estimated the minimum deep CO_2 outgassing yield (1.24×10^4 t C yr^{-1}) based on DIC flux corrected for outgassing by a Rayleigh model. In the Changbaishan volcanic area, deep carbon release flux was higher than CO_2 consumption flux by silicate weathering, while the deep CO_2 outgassing flux was an underestimate, consistent with the hypothesis that deep CO_2 release regulates climate on geological timescales. This study calls for a better understanding of the effects of volcanic activities on Earth's surface carbon cycling, which has great implications on studying global climate change.

Plain Language Summary The balance between volcanic degassing and silicate weathering may control the atmospheric CO_2, regulating long-term global climate. Volcanic areas have attracted large amounts of attentions, because of its intricate effects on atmospheric CO_2. We investigated water chemistry, $\delta^{13}C_{DIC}$ and $\Delta^{14}C_{DIC}$ in Changbaishan volcanic area to understand carbon biogeochemical processes in volcanic areas. In most previous studies, $\delta^{13}C_{DIC}$ was used to trace the sources of DIC in volcanic areas, but this study evidenced that $\delta^{13}C_{DIC}$ is highly controlled by CO_2 outgassing, bringing great uncertainties on source discrimination. $\Delta^{14}C_{DIC}$ is non-sensitive to CO_2 outgassing, so we used $\Delta^{14}C_{DIC}$ to trace the sources of DIC. Based on the Rayleigh fractionation model, $\delta^{13}C_{DIC}$ was used to estimate the minimum CO_2 outgassing fluxes in this study area. At last, we evaluated the net carbon budget concerning deep carbon release and silicate weathering, and found that deep carbon release flux was higher than CO_2 consumption flux by silicate weathering. This study highlights the effects of deep carbon release on Earth's surface and provides mechanistic insights into carbon biogeochemical processes in volcanic areas.

Key Points:

- The water chemical compositions and isotopic compositions of DIC varied in a wide range in Changbaishan volcanic rivers
- The hydrothermal fluids had a significant impact on solutes budgets, as well as carbon isotopes for the volcanic rivers
- Deep carbon release flux was higher than CO_2 consumption flux by silicate weathering in Changbaishan volcanic area

Supporting Information:

Supporting Information may be found in the online version of this article.

Correspondence to:

S.-L. Li and S. Xu,
siliang.li@tju.edu.cn;
sheng.xu@tju.edu.cn

Citation:

Zhong, J., Wang, L., Caracausi, A., Galy, A., Li, S.-L., Wang, W., et al. (2023). Assessing the deep carbon release in an active volcanic field using hydrochemistry, $\delta^{13}C_{DIC}$ and $\Delta^{14}C_{DIC}$. *Journal of Geophysical Research: Biogeosciences*, *128*, e2023JG007435. https://doi.org/10.1029/2023JG007435

Received 10 FEB 2023
Accepted 30 MAR 2023

Author Contributions:

Conceptualization: Jun Zhong, Cong-Qiang Liu, Sheng Xu
Formal analysis: Jun Zhong, Linan Wang, Wanfa Wang, Maoliang Zhang
Funding acquisition: Si-Liang Li, Sheng Xu
Investigation: Jun Zhong, Linan Wang, Wanfa Wang, Maoliang Zhang, Guo-Ming Liu
Methodology: Jun Zhong, Antonio Caracausi, Albert Galy, Si-Liang Li
Project Administration: Sheng Xu
Supervision: Si-Liang Li
Writing – original draft: Jun Zhong
Writing – review & editing: Jun Zhong, Antonio Caracausi, Albert Galy, Si-Liang Li, Cong-Qiang Liu, Sheng Xu

1. Introduction

Volcanic activities are thought to have great implications on regional and global carbon cycles (Chiodini et al., 2020; W. C. Evans et al., 2004; James et al., 1999; Seward & Kerrick, 1996). A quantification of the input of deep carbon to the Earth's surface is crucial to understand the carbon budget and carbon biogeochemical processes in active volcanic zone (Caudron et al., 2012; Chiodini et al., 2020; Rivé et al., 2013). It is commonly known that the volcanic eruptions would release a large amount of CO_2 into the atmosphere, which can regulate the climate at the geological timescales (Berner & Caldeira, 1997; Hilton & West, 2020). Recently, it has been recognized that

large amounts of CO_2 are degassed from volcanic areas long after eruptions, and the effects of solid Earth CO_2 release would persist for a long time (Caracausi et al., 2015; Chiodini et al., 2020; Kis et al., 2017).

Deep carbon emission dissolved in waters makes a significant contribution to both the river carbon budget and the total mantle CO_2 release budget in volcanic areas (Caracausi et al., 2015; W. C. Evans et al., 2004; Rivé et al., 2013). And the deep CO_2 involved in chemical weathering reactions would add uncertainties in the calculation of atmospheric CO_2 consumption (Dessert et al., 2009; Li et al., 2016; Rivé et al., 2013). Investigating the sources of dissolved inorganic carbon (DIC) in volcanic catchments and the impact of deep carbon release on river DIC budget have significant implications on evaluating the regional carbon balance between CO_2 consumption by silicate weathering and deep carbon refilling in the shallow layer of the volcanic plumbing systems and in atmosphere. In addition, deep CO_2 degassing is considered as an important natural carbon source and considered to exceed CO_2 consumption by silicate weathering in active tectonic and volcanic areas (Gaillardet & Galy, 2008; Perez et al., 2011; Svensen & Jamtveit, 2010). Therefore, the deep carbon contributions (i.e., dissolved and gaseous state) to the Earth's surface in volcanic areas need to be assessed to understand the full carbon biogeochemical cycle.

In respect to the deep carbon contributions, chemical mass-balance approaches provide viable ways to the measurement of fluxes and have significant advantages of accounting for hydrothermal carbon fluxes (Becker et al., 2008; Caracausi et al., 2015; Zhong et al., 2022). Radiocarbon (^{14}C) is considered to be the most reliable and universal indicator of geological "dead carbon" contribution (W. C. Evans et al., 2004; Genereux et al., 2009; James et al., 1999; Mao et al., 2018; Stefánsson et al., 2016). Because the deep ^{14}C-free carbon ($\Delta^{14}C = -1{,}000‰$) can mix with surface modern carbon ($\Delta^{14}C = \sim 0‰$), the $\Delta^{14}C$ value of DIC ($\Delta^{14}C_{DIC}$) in rivers and groundwaters can be used to constrain these two sources. $\delta^{13}C_{DIC}$ value is highly affected by CO_2 outgassing through the Rayleigh distillation process (Barbieri et al., 2020; Becker et al., 2008; M. J. Evans et al., 2008; Menzies et al., 2018), so it can express the CO_2 outgassing processes. While $\Delta^{14}C_{DIC}$ is non-sensitive to CO_2 outgassing (Marwick et al., 2015; Mayorga et al., 2005; Zhong et al., 2021), and it is conservative during the mixing process. Therefore, coupling $\delta^{13}C_{DIC}$ and $\Delta^{14}C_{DIC}$ can be useful to constrain the carbon physical and biogeochemical processes in active volcanic catchments.

Changbaishan (a.k.a. Tianchi, Baitoushan, or Baegdusan) volcano has been volcanically active for at least 2.7 Ma (Hahm et al., 2008 and references therein), and the lasted eruption occurred in 1903 CE (Zhang et al., 2015 and references therein). Importantly, it has abundant hydrothermal activities and releases large amounts of mantle CO_2 (Hahm et al., 2008). Therefore, Changbaishan volcanic area should be a prime area to investigate the impacts of deep carbon on carbon cycling in the Earth's surface. In this study, we analyzed the concentrations of major ions, $\delta^{13}C_{DIC}$ and $\Delta^{14}C_{DIC}$ of rivers, cold springs, hot springs, and crack rivers (i.e., running water in narrow and deep tension cracks of cold lava flows and volcanic edifices) in Changbaishan volcanic area. The objectives of this study are to (a) constrain the deep carbon contribution to the river waters; (b) estimate the deep CO_2 outgassing fluxes; and (c) evaluate the net carbon budget induced by silicate weathering versus deep carbon release in the Changbaishan volcanic area.

2. Methods

2.1. Study Area

The Changbaishan area is located in Northeast China, on the northern margin of the Archean-Proterozoic Sino-Korean craton (Figure 1a; Hahm et al., 2008; Sun et al., 2020). Tianchi, an active volcanic crater lake on the boundary between China and North Korea (Figures 1a and 1b), and main Changbaishan volcanic activities are concentrated in this region (Hahm et al., 2008; Sun et al., 2020; Yan et al., 2017). It includes the headwaters of Songhua River, Yalu River, and Tumen River. During the Holocene, Changbaishan Tianchi volcano has erupted several times, resulting in the formation of the 384-m-deep and 5-km-wide Tianchi crater that hosts the lake (Zhu et al., 1981). The last eruption in 1903 formed pyroclastic deposits around the Changbaishan Tianchi crater (Wei et al., 2013; Yan et al., 2017; Zhang et al., 2015). Importantly, Tianchi lake releases large amounts of CO_2 due to active degassing of volatiles (Hahm et al., 2008; Shangguan et al., 1997; Sun et al., 2020). Obvious hydrothermal activities also occur beyond the Tianchi crater lake in this area. For instance, there are many hot springs (Figures 1c and 1d) occurring in the Julong hydrothermal system and Jinjiang hydrothermal system (Wei et al., 2013; Zhang et al., 2015).

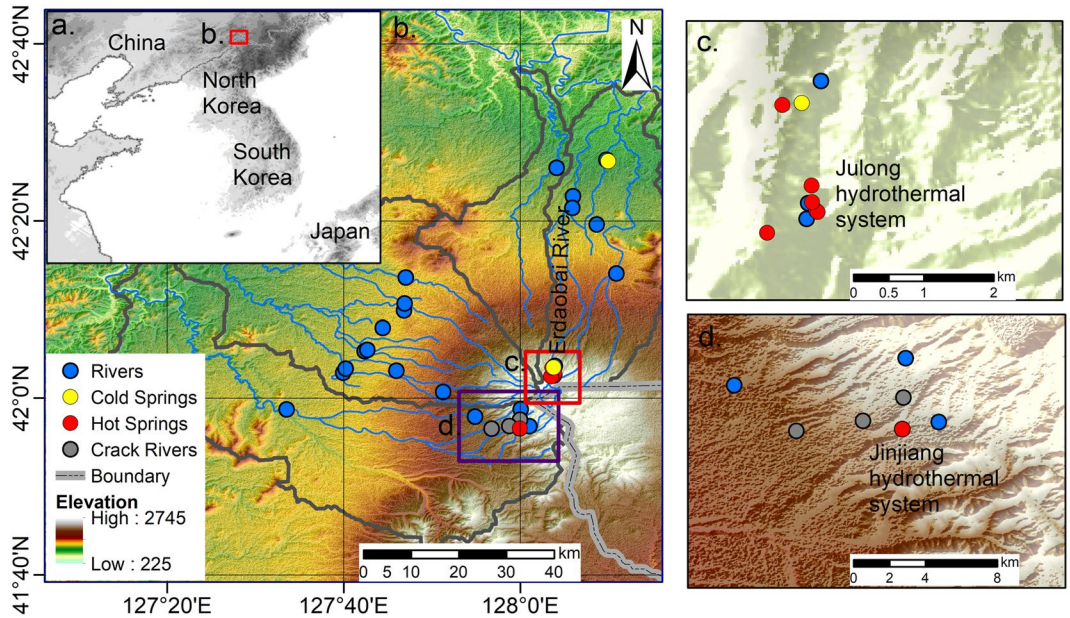

Figure 1. (a) The location of the study area. (b) Map showing the sampling sites of rivers, hot springs, cold springs, and crack rivers (running water in narrow and deep tension cracks of cold lava flows and volcanic edifices) in this study. (c) and (d) represent the sample sites near the Tianchi crater lake in the north and west edges of the Changbaishan volcanic area.

The basement of the Changbaishan region consists of Paleozoic strata, predominantly Mesozoic granite, and Archean to middle-late Proterozoic metamorphic rocks (Hahm et al., 2008). The eruptive history of Tianchi volcano can be grouped into three stages according to different eruptive products: eruptions from the Miocene to the Early Pleistocene produced Alkali and tholeiitic basalts that cover an area of 7,200 km^2; eruptions during the cone formation stage produced the youngest shield basalts near the Tianchi cone, which are overlain by thick alkali trachytes; and comenditic pyroclastic deposits occurred at the late eruption stage.

The outlet of Tianchi lake is located in the northern edge of the Changbaishan mountain, which is the origin of the Erdaobai River (Figure 1b). There are some narrow and deep crack rivers in the western edge of the Changbaishan mountain (Figure 1b). There are no evaporites and carbonate outcropping observed in the studied area (Hahm et al., 2008). The climate of the studied area is characterized by a temperate continental climate, with long and cold winter, and short and cool summer which accounts for more than half of the annual precipitations (Yan et al., 2017). The mean annual precipitation ranges from 700 to 900 mm, with the maximum value at the summit of the Changbaishan Tianchi volcano. The mean annual temperature varies from −7.3°C to 3.0°C in the studied area, with the lowest temperature occurring at the summit of Tianchi lake (Zhu et al., 1981).

2.2. Sampling and Field Measurement

Field investigation and sampling were conducted in September 2019 and October 2020. We collected the waters from (a) the rivers from the northern and western sides of the Tianchi crater lake ($n = 26$), (b) cold springs ($n = 2$), (c) crack river ($n = 3$), and (d) Julong hot springs and Jinjiang hot springs ($n = 7$; Figures 1b–1d). For the rivers, we sampled the Erdaobai River at the headwater (i.e., the outlet water of Tianchi lake) and several downstream locations, and we also sampled all tributaries rivers that flow to Tianchi crater lake. Water temperature, pH, and electrical conductivity (EC) were determined in situ with a multiparameter profiler (WTW, pH3630, Germany). The water samples were filtered with 0.45 μm fiber filters, and subsequently stored at 4°C before analyses.

2.3. Analytical Methods

Total alkalinity was determined by titration with 0.02 mol L^{-1} hydrochloric acid after sampling within 24 hr (Zhong et al., 2018), and DIC concentration was calculated based on mass action relationships and the relative equilibrium constants. All laboratory analyses for water samples were conducted in the School of Earth System

Science, Tianjin University. Major anion concentrations were analyzed by ion chromatography (Dionex ICS90, USA), and major cation concentrations were measured using an inductively coupled plasma-optical emission spectrometer (Agilent 5110 ICP-OES, USA) after acidification to pH of 2–3 using ultra-purified HNO_3, both of which have overall uncertainties ≤5%.

For the determination of $\delta^{13}C_{DIC}$ and $\Delta^{14}C_{DIC}$, water samples were first injected into a vacuum bottle with 85% phosphoric acid and a bar magnet by a syringe. Subsequently, the produced CO_2 was extracted and cryogenically purified in a vacuum system (Zhong et al., 2018 and references therein). After CO_2 purification, $\delta^{13}C_{DIC}$ was measured using an isotope ratio mass spectrometer (Finnigan MAT 253 plus, Germany), and expressed in ‰ notation with respect to the international V-PDB standard. Repeat measurements of a working standard suggest the overall uncertainty of ±0.1‰. For analysis of the $\Delta^{14}C$, part of the above purified CO_2 was graphitized using the sealed tube zinc reduction method (Xu et al., 2007). The $^{14}C/^{12}C$ ratio was determined using a 0.5 MV accelerator mass spectrometer (AMS; Dong et al., 2018). Repeated measurements of the secondary standards showed a ~0.3% precision and accuracy on $^{14}C/^{12}C$ ratio. The $\Delta^{14}C_{DIC}$ values were reported to correct for mass-dependent isotopic fractionation effects using the online AMS-measured $\delta^{13}C$ values.

3. Results

3.1. Chemical Compositions of Water Samples

The analytical results are shown in Table 1. The pH values of the river waters varied in a narrow range from 7.28 to 8.30. Major ion concentrations (except NO_3^-) varied in extremely wide ranges; for example, Na^+ was the most abundant cation, ranging from 90 to 2,940 μmol L^{-1}; Ca^{2+} varied from 95 to 302 μmol L^{-1}, and Mg^{2+} ranged from 23 to 248 μmol L^{-1}; the DIC concentrations ranged from 170 to 2,868 μmol L^{-1} with an average of 953 μmol L^{-1}. For most of the solutes, the highest values were spatially observed in the headwaters of the Erdaobai River from the outlet of Tianchi lake. Low NO_3^- values were observed in all rivers, ranging from 7 to 95 μmol L^{-1} with an average of 47 μmol L^{-1}, consistent with negligible anthropogenic activities.

Most of the ions in cold springs were much lower than those in most rivers (Table 1). On the other hand, most of the ions, except NO_3^- (18–448 μmol L^{-1}), were much higher in the hot springs than those in rivers and cold springs, with Ca^{2+} of 2,908–8,238 μmol L^{-1}, Mg^{2+} of 58–91 μmol L^{-1}, and Na^+ of 4,863–16,955 μmol L^{-1} (Table 1). These high cations values are also associated with high DIC values varying from 4,454 to 20,317 μmol L^{-1} (Table 1). In addition, most ions in crack rivers showed lower concentrations than those in hot springs but higher concentrations than those in rivers and cold springs (Table 1). The ions in the Tianchi lake were similar to those in the crack rivers, and did not show significant spatial-temporal variations (Zhu et al., 1981).

The river Ca^{2+}/Na^+ and Mg^{2+}/Na^+ ratios varied from 0.103 to 1.715 and from 0.012 to 0.749, respectively (Figure 2a), with the lowest values at the headwater of the Erdaobai River. Furthermore, the Ca^{2+}/Na^+ and Mg^{2+}/Na^+ ratios of cold springs overlap the range of those in rivers (Figure 2a). The Ca^{2+}/Na^+ and Mg^{2+}/Na^+ ratios of the hot springs ranged from 0.047 to 0.106 and from 0.005 to 0.033, respectively, which were much lower than those in river waters (Figure 2a). The Ca^{2+}/Na^+ and Mg^{2+}/Na^+ ratios of the Tianchi lake and crack rivers had low values, similar to the headwater of the Erdaobai River. All these samples had lower Ca^{2+}/Na^+ and Mg^{2+}/Na^+ ratios than those in most global large rivers (Gaillardet et al., 1999).

The spatial variations of Ca^{2+}/Na^+ ratio followed an inverse relationship with concentrations of most solutes in the studied area, shown by the negative power-law correlation between DIC and Ca^{2+}/Na^+ ratios for all the samples (Figure 2b).

3.2. Isotopic Compositions of DIC

The $\delta^{13}C_{DIC}$ and $\Delta^{14}C_{DIC}$ values of the river waters in the region of Changbaishan volcano showed a wide range of variability, varying from −14.1‰ to 3.5‰ and from −832‰ to 22‰, respectively (Table 1). The river $\delta^{13}C_{DIC}$ values were much higher and $\Delta^{14}C_{DIC}$ values were much lower than those in most global rivers, but comparable to rivers in other volcanic areas (Figure 3). For volcanic areas, the $\delta^{13}C_{DIC}$ in Volcan Barva had much lower values than those in this study (Genereux et al., 2009), while Ukinrek Maars showed much higher $\delta^{13}C_{DIC}$ (W. C. Evans et al., 2009). For the hot springs, the DIC was ^{13}C-enriched, having $\delta^{13}C$ values from −2.2‰ to 3.0‰, and ^{14}C-depleted, with $\Delta^{14}C$ values varying from −998‰ to −947‰. Similar to hot springs, crack rivers

Table 1
Chemical and Isotopic Compositions of Water for Rivers, Cold Springs, Hot Springs and Crack Rivers in Changbaishan Volcanic Area

Nos.	Types	Date	Longitude (°E)	Latitude (°N)	pH	EC (μs cm^{-1})	Ca^{2+} (μmol L^{-1})	K^{+} (μmol L^{-1})	Mg^{2+} (μmol L^{-1})	Na^{+} (μmol L^{-1})	SO_4^{2-} (μmol L^{-1})	Cl^{-} (μmol L^{-1})	NO_3^{-} (μmol L^{-1})	DIC (μmol L^{-1})	$\delta^{13}C_{DIC}$ (‰)	$\Delta^{14}C_{DIC}$ (‰)
R1	River	2019/09/22	128.07	42.06	8.30	337	302	161	35	2,940	62	529	25	2,868	2.6	−808
R2	River	2019/09/22	128.06	42.04	8.01	283	282	146	34	2,377	60	438	27	2,446	3.5	−816
R3	River	2019/09/22	128.06	42.05	7.90	306	295	153	34	2,620	62	479	26	2,685	2.7	−832
R4	River	2019/09/23	128.18	42.23	7.54	79	109	74	53	431	69	37	29	573	−8.8	3
R5	River	2019/09/23	128.14	42.33	7.51	101	135	75	142	434	70	45	19	836	−12.6	−61
R6	River	2019/09/23	128.10	42.38	7.94	184	183	102	99	1,340	71	217	31	1,541	−3.8	−405
R7	River	2019/09/23	128.10	42.36	7.73	200	198	110	100	1,500	68	244	21	1,711	−3.3	−446
R8	River	2019/09/23	128.16	42.45	7.39	140	250	84	248	447	97	53	7	1,359	−12.1	−138
R9	River	2019/09/23	128.07	42.43	7.59	84	129	57	101	349	65	44	44	655	−10.5	−140
R10	River	2020/11/22	128.00	41.94	7.44	96	114	55	38	661	34	63	48	939	−3.3	−752
R11	River	2020/11/22	128.00	41.94	7.36	50	104	44	24	263	31	25	51	336	−2.9	−412
R12	River	2020/11/22	128.02	41.95	7.28	31	95	40	25	96	24	15	45	210	−5.4	−4
R13	River	2020/11/22	128.00	41.98	7.52	34	116	30	23	90	36	16	49	170	−10.3	−65
R14	River	2020/11/23	127.86	42.01	7.37	55	184	34	35	163	46	18	59	315	−9.2	−50
R15	River	2020/11/23	127.92	41.97	8.12	37	158	35	32	92	24	15.9	60	325	−9.7	19
R16	River	2020/11/23	127.77	42.05	7.55	74	167	54	58	311	43	34	46	632	−9.3	14
R17	River	2020/11/23	127.67	42.05	7.45	63	163	41	49	206	45	21	47	424	−7.9	−40
R18	River	2020/11/23	127.67	42.10	7.60	85	156	51	90	363	38	42	51	796	−6.6	−223
R19	River	2020/11/23	127.56	41.98	7.95	99	175	54	84	513	33	51	41	921	−5.5	−218
R20	River	2020/11/23	127.67	42.06	8.00	128	202	73	232	448	25	47	48	1,399	−12.1	−391
R21	River	2020/11/23	127.71	42.09	7.66	68	146	56	69	263	38	35	79	532	−7.8	−120
R22	River	2020/11/23	127.71	42.09	7.44	58	134	54	68	174	37	20	76	436	−8.8	−38
R23	River	2020/11/23	127.74	42.13	7.71	94	213	51	162	216	28	26	59	982	−14.1	−114
R24	River	2020/11/23	127.78	42.16	7.72	67	182	43	93	160	26	27	55	604	−11.6	22
R25	River	2020/11/23	127.78	42.18	7.55	62	152	50	66	186	46	23	95	448	−7.9	19
R26	River	2020/11/23	127.78	42.23	8.70	72	158	48	103	229	38	24	79	636	−12.7	−91
C1	Cold Spring	2020/11/24	128.06	42.06	7.74	35	125	42	24	122	29	21	61	178	−6.3	−225
C2	Cold Spring	2019/09/23	128.17	42.45	6.88	99	110	78	170	405	46	36	22	1,221	−9.2	−478
H1	Hot Spring	2019/09/22	128.07	42.04	6.82	1,576	823	525	91	16,955	207	3,140	18	20,317	−2.2	−992
H2	Hot Spring	2019/09/22	128.07	42.04	6.97	1,567	775	510	90	16,574	230	3,042	35	18,853	−1.6	−994
H3	Hot Spring	2019/09/22	128.06	42.05	8.22	814	454	289	68	8,190	147	1,374	38	7,848	1.0	−973
H4	Hot Spring	2019/09/22	128.06	42.05	8.47	525	290	197	58	4,863	103	981	47	4,454	2.1	−947
H5	Hot Spring	2020/11/24	128.06	42.04	6.66	1,638	913	468	66	15,605	31	3,522	65	8,810	0.1	−999
H6	Hot Spring	2020/11/24	128.06	42.06	6.40	764	669	287	96	6,284	44	988	93	6,400	3.0	−985
H7	Hot Spring	2020/11/22	128.00	41.94	6.83	1,704	762	765	521	15,651	222	1,967	4	23,528	−0.4	−996
CR1	Crack River	2020/11/23	128.00	41.96	8.05	212	211	70	24	1,692	41	196	47	2,153	−0.8	−849
CR2	Crack River	2020/11/23	127.98	41.95	7.52	259	242	86	31	2,037	41	237	49	2,700	−2.0	−905
CR3	Crack River	2020/11/23	127.95	41.94	8.54	295	270	92	31	2,376	44	284	47	2,949	−0.8	−782

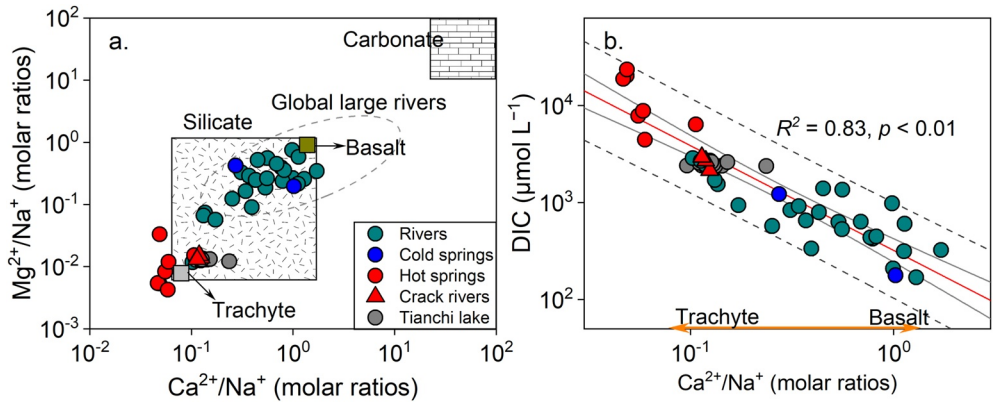

Figure 2. (a) The relationship between Mg^{2+}/Na^{+} ratios and Ca^{2+}/Na^{+} ratios, with end-members of silicate and carbonate from Gaillardet et al. (1999). Data of Tianchi lake were from Zhu et al. (1981). The dark-gray dashed ellipse represents the range of large rivers (Gaillardet et al., 1999). The end-members of basalt and trachyte are from Andreeva et al. (2014) and Table S1 in Supporting Information S1. (b) The negative power-law relationship between dissolved inorganic carbon (DIC) and Ca^{2+}/Na^{+} ratios. The red solid line represents the linear regression for all the water samples analyzed in this study, with the dark solid lines and the dark dashed lines corresponding to areas of 95% confidence and 95% prediction intervals, respectively.

had ^{13}C-enriched and ^{14}C-depleted DIC values, ranging from −2.0‰ to −0.8‰ and −905‰ to −783‰, respectively. However, the DIC in cold spring water was characterized by lower $\delta^{13}C_{DIC}$ values (−6.3‰ and −9.2‰) and higher $\Delta^{14}C_{DIC}$ values (−225‰ and −478‰). In fact, most $\delta^{13}C_{DIC}$ values of hot springs showed much higher values than those in river waters, whereas all $\Delta^{14}C_{DIC}$ values of the hot waters were much lower and close to dead carbon ($\Delta^{14}C_{DIC} = -1{,}000‰$) values.

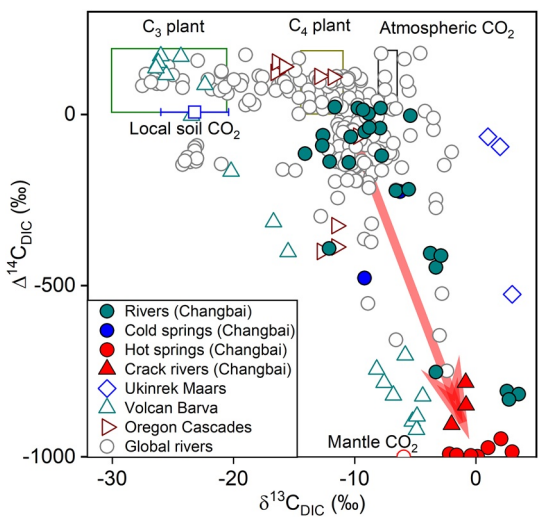

Figure 3. Plot of $\Delta^{14}C_{DIC}$ versus $\delta^{13}C_{DIC}$. Data of the global rivers, and end-members of C_3 plants, C_4 plants, and atmospheric CO_2 were from Marwick et al. (2015). $\delta^{13}C$ values of local soil CO_2 (−25.6‰ to −16.3‰) and gas CO_2 (−7.2‰ to −3.5‰) in hot springs were from Sun et al. (2020) and Hahm et al. (2008), respectively. $\Delta^{14}C_{DIC}$ and $\delta^{13}C_{DIC}$ of rivers in volcanic areas (i.e., Ukinrek Maarrs, Volcan Barva, and Oregon Cascades) were from W. C. Evans et al. (2009), Genereux et al. (2009), and James et al. (1999). The $\delta^{13}C_{DIC}$ of hot springs (red solid circles) are (a) higher than that of gas CO_2 in hot springs and (b) variable, ascribing to the effect of carbon isotopic fractionation by the degassing of different amounts. The red arrow represents the effects of hydrothermal fluids on carbon isotopes.

4. Discussion

4.1. Direct Hydrothermal Fluxes in the Catchments

4.1.1. Solute Sources of River and Spring Waters

Dissolved ions in rivers draining active volcanic areas have two main sources: low-temperature weathering products and hydrothermal fluids (i.e., high-temperature weathering products; e.g., Caracausi et al., 2015; Chiodini et al., 2011; Rivé et al., 2013). The ratios of the major ions are useful tools for determining the solute sources, and allow to recognize the weathering of different lithologies (Gaillardet et al., 1999; Zhong et al., 2018). The waters in crack rivers and Tianchi lake have similar chemical characteristics with hot springs (Figure 2a), supporting a high contribution of hydrothermal fluids for those areas. The low Ca^{2+} concentrations and Ca^{2+}/Na^{+} ratios (0.103–1.715) in the river waters support that carbonate weathering contribution is negligible in this study area. This is in a good agreement with the local lithology that is not characterized by the presence of carbonate (Hahm et al., 2008; Shangguan et al., 1997). Water chemistry of hydrothermal fluids in the Changbaishan volcanic area is from high-temperature silicate dissolution, which shows lower Ca^{2+}/Na^{+} and Mg^{2+}/Na^{+} ratios than those in low-temperature silicate weathering (Bai et al., 2017). The negative relationship between DIC concentrations and Ca^{2+}/Na^{+} ratios for all the samples shows the mixing between fluids corresponding to high-temperature silicate dissolution and those of low-temperature silicate weathering (Figure 2b).

The Ca^{2+}/Na^{+} and Mg^{2+}/Na^{+} ratios of the rivers and cold springs fall into the field of silicate, but these ratios are different in volcanic rocks such as the basalt and trachyte that constitute the flanks and the volcanic cone of

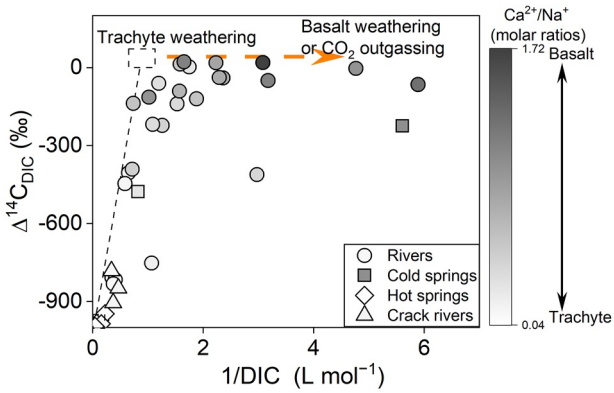

Figure 4. The correlation between $\Delta^{14}C_{DIC}$ and 1/DIC ratio. The dashed black line represents the mixing of high-temperature silicate dissolution and potential low-temperature silicate weathering (mainly trachyte weathering), and the dashed orange arrow represents the effects of CO_2 outgassing and basalt weathering. The shades of grays indicate the variation in Ca^{2+}/Na^+ ratio, where dark represents high values (basalt) and light represents low values (trachyte).

Changbaishan volcano, respectively (Figure 2a). The trachyte is characterized by low Ca^{2+}/Na^+ and Mg^{2+}/Na^+ ratios, similar to hot springs, whereas basalt has high Ca^{2+}/Na^+ and Mg^{2+}/Na^+ ratios (Andreeva et al., 2014; Bai et al., 2017; Table S1 in Supporting Information S1). However, the Ca^{2+}/Na^+ ratios in the dissolved phases are also sensitive to the different weathering kinetics of Ca-rich and Na-rich phases, complicating further the constraint of carbon sources (Bai et al., 2017).

4.1.2. $\Delta^{14}C_{DIC}$ as a Tracer of Hydrothermal Carbon in the Volcanic Catchments

As discussed above, the DIC in rivers and cold springs are mainly from high-temperature silicate dissolution and low-temperature silicate weathering. Under high-temperature water/rock conditions, the produced DIC is transported to rivers by hydrothermal fluids, with high DIC concentrations, high $\delta^{13}C_{DIC}$ and low $\Delta^{14}C_{DIC}$ (Genereux et al., 2009; Stefánsson et al., 2016). Low-temperature silicate weathering involves biogenic CO_2 that produces low concentrations DIC, with low $\delta^{13}C_{DIC}$ and high $\Delta^{14}C_{DIC}$ (Genereux et al., 2009; Marwick et al., 2015; Stefánsson et al., 2016). Whereas high-temperature silicate dissolution involves deep CO_2 and produces DIC with characteristics of deep CO_2 (Rivé et al., 2013). In this study area, the soil CO_2 is mainly from biogenic sources (Sun et al., 2020), so we neglect the role of deep CO_2 on low-temperature silicate wreathing. The low $\Delta^{14}C_{DIC}$ values (i.e., aged DIC) in the volcanic catchments (Figure 3) indicate that deep carbon is an important source for DIC in rivers, cold springs, and crack rivers. As $\Delta^{14}C_{DIC}$ is insensitive to mass-dependent fractionation during CO_2 degassing (Zhong et al., 2021), it can be mainly affected by the mixing of deep carbon and Earth's surface modern carbon. However, there is no strong linear relationship predicted by Keeling (1958) between $\Delta^{14}C_{DIC}$ and 1/DIC ratios (Figure 4). Young DIC (high $\Delta^{14}C_{DIC}$ values) can have a wide range of DIC concentration (hence a large variation in 1/DIC, Figure 4), with higher Ca^{2+}/Na^+ ratios for higher 1/DIC values (Figures 2b and 4). The plot of $\Delta^{14}C_{DIC}$ versus Ca^{2+}/Na^+ ratios shows that most of the samples can be explained with the three end-members: hydrothermal fluids, basalt, and trachyte (Figure S1 in Supporting Information S1). The fluids corresponding to the basalt and trachyte end-members are characterized by young DIC, indicating that low-temperature weathering affects different silicate rocks. In addition, CO_2 outgassing (the release of CO_2 from water) would not significantly shift the $\Delta^{14}C_{DIC}$, but increase the 1/DIC ratios, which also can cause the large variations in 1/DIC ratios for young DIC. Briefly, weathering of different silicate rocks, CO_2 outgassing, and hydrothermal fluids control the solutes' dynamics.

The export of deep CO_2 as river DIC should be added to the deep carbon flux; otherwise, the deep carbon release fluxes would be underestimated (Dessert et al., 2009; Rivé et al., 2013). $\Delta^{14}C_{DIC}$ is conservative in biogeochemical processes, evidenced by the fact that most of the samples are located near the mixing line for $\Delta^{14}C_{DIC}$ and Cl^- (Figure S2 in Supporting Information S1). Isotopic mass-balance equation was used to quantify the fractions of hydrothermal DIC and modern DIC in waters as follows:

$$\Delta^{14}C_{DIC} = \left(1 - f_{Hyd}\right) \times \Delta^{14}C_{Mod} + f_{Hyd} \times \Delta^{14}C_{Hyd}, \quad (1)$$

where f_{Hyd} is the fraction of hydrothermal carbon, and the term $(1 - f_{Hyd})$ represents the fraction of modern carbon. $\Delta^{14}C_{DIC}$, $\Delta^{14}C_{Mod}$, and $\Delta^{14}C_{Hyd}$ are the $\Delta^{14}C$ values of measured DIC, modern carbon, and deep carbon (−1,000‰), respectively.

In this calculation, we assumed that the $\Delta^{14}C_{Mod}$ is the highest $\Delta^{14}C_{DIC}$ (22‰) measured in rivers, consistent with the modern atmospheric CO_2 observations (Niu et al., 2016). The calculated f_{Hyd} resulted in a wide range from 0% to 84% for the rivers, and 24% and 49% for the cold springs. The calculated f_{Hyd} of crack rivers showed high values, ranging from 79% to 91%. Based on the calculated f_{Hyd}, the hydrothermal DIC flux (DIC_{Hyd} flux) and modern DIC flux (DIC_{Mod} flux) can be estimated as below:

$$DIC_{Hyd}\,flux = f_{Hyd} \times DIC \times Discharge, \quad (2)$$

$$DIC_{Mod}\,flux = \left(1 - f_{Hyd}\right) \times DIC \times Discharge, \quad (3)$$

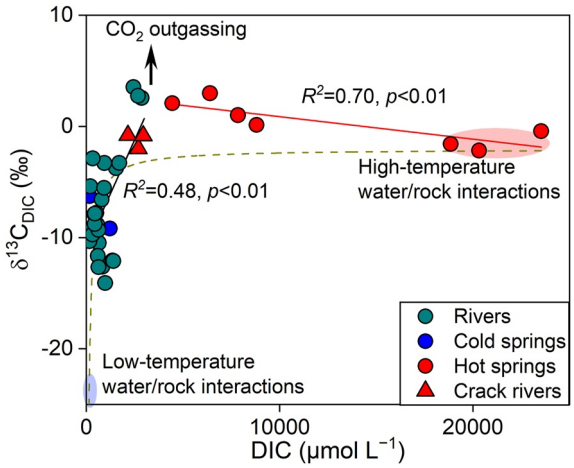

Figure 5. Correlation between $\delta^{13}C_{DIC}$ and dissolved inorganic carbon (DIC) concentration for the water samples. The black and red solid lines are the linear regression models for rivers and hot springs, respectively. The dashed line represents the theoretical mixing line of high-temperature water/rock interaction and low-temperature water/rock interaction.

In this study, we estimated the carbon fluxes using discharges from Lai (2019) and Lin (2016), and average measured DIC concentrations and $\Delta^{14}C_{DIC}$. The DIC_{Hyd} flux is 0.33×10^4 t C yr^{-1}, whereas the DIC_{Mod} flux is 1.51×10^4 t C yr^{-1} for the studied area. These values correspond to a yield of 0.79 and 3.60 t C yr^{-1} km^{-2}, respectively.

4.2. Deep CO_2 Degassing in the Changbaishan Volcanic Field

The relationship between $\delta^{13}C_{DIC}$ and DIC does not follow the mixing line of hydrothermal fluids and low-temperature silicate weathering (Figure 5), suggesting that $\delta^{13}C_{DIC}$ is not simply affected by mixing process. There were two contrary patterns between $\delta^{13}C_{DIC}$ and DIC for rivers and hot springs, that is, a positive linear relationship for rivers but a negative linear correlation for hot springs (Figure 5). For the hot springs, low DIC concentrations could be attributed to (a) the dilution by surface water, and (b) the loss of DIC through CO_2 outgassing that is characterized by elevated $\delta^{13}C_{DIC}$ values related to the carbon isotopic fractionation during CO_2 outgassing (Barbieri et al., 2020; Becker et al., 2008; Chiodini et al., 2004, 2020; Lewicki et al., 2013; Menzies et al., 2018; Mook et al., 1974). The positive relationship between $\delta^{13}C_{DIC}$ and DIC in rivers (Figure 5) mainly reflects the mixing between the ^{13}C-enriched deep DIC and ^{13}C-depleted surface biogenic DIC. In addition, rivers with high contributions of deep DIC seem to experience intense CO_2 outgassing, producing high $\delta^{13}C_{DIC}$ (Figures 5 and 6a). Thus, it can be concluded that mixing and CO_2 outgassing are two primary processes controlling the carbon dynamics in active volcanic catchments (Figure 6a).

CO_2 outgassing significantly occurs in the Tianchi crater lake and hot springs (Zhang et al., 2015). The loss of carbon through CO_2 outgassing will largely shift the $\delta^{13}C_{DIC}$ values, according to the Rayleigh distillation process (e.g., Becker et al., 2008; M. J. Evans et al., 2008). Open system CO_2 outgassing at temperatures below 125°C progressively increases the $\delta^{13}C_{DIC}$, because $^{12}CO_2$ diffuses faster than $^{13}CO_2$ (M. J. Evans et al., 2008; Polsenaere & Abril, 2012). Complexities in multi-stage processes of generation and transport of CO_2, as well as the sensitivity of temperature-dependent carbon-isotope fractionation factor, increase the difficulty in constraining deep CO_2 outgassing flux, and it is only possible to model the minimum deep CO_2 outgassing flux (Becker et al., 2008). Carbon isotopes fractionation by CO_2 outgassing in an open system can be modeled by a Rayleigh process (M. J. Evans et al., 2008):

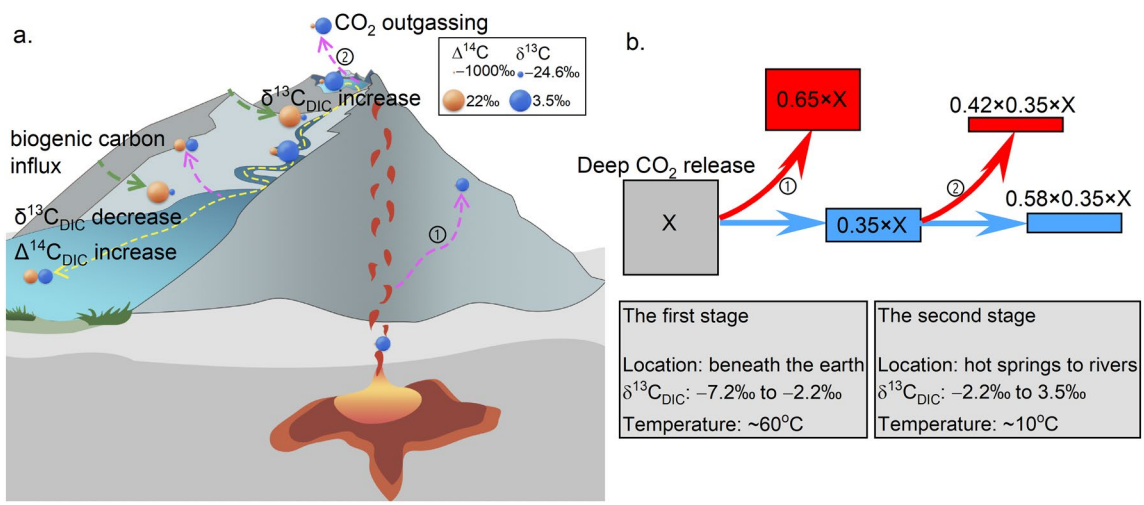

Figure 6. (a) Schematic model of the Changbaishan volcanic CO_2 degassing and carbon in-stream processes. The sizes of the blue and orange spheres represent the values of $\delta^{13}C$ and $\Delta^{14}C$, respectively. The yellow arrow represents the fluvial dissolved inorganic carbon (DIC) in the river. The magenta arrows represent the CO_2 outgassing, and olive arrows denote the biogenic carbon influx. (b) Calculation processes and calculated DIC proportions in CO_2 outgassing in the Changbaishan volcanic fields. *X* represents the total deep carbon release. The red arrows and frames represent the CO_2 outgassing, whereas the blue arrows and frames represent fluvial DIC transport. ① and ② represent the first and second stages of CO_2 outgassing for both (a) and (b).

$$R_{DIC} = R^{0}_{DIC} \times f_{DIC}^{(1/\alpha-1)} \quad (4)$$

where R_{DIC} and R^{0}_{DIC} are the carbon isotope ratio of DIC after outgassing and in initial fluid, respectively, f_{DIC} is the fraction of the remaining DIC after CO_2 outgassing, and α is the temperature-dependent fractionation factor between aqueous HCO_3^- and gaseous CO_2 (Mook et al., 1974). According to Alling et al. (2012), Equation 4 can be modified as follows:

$$\delta^{13}C_{fin} = \delta^{13}C_{ini} + 10^3 \times (\alpha - 1) \times \ln(f_{DIC}), \quad (5)$$

where $\delta^{13}C_{fin}$ and $\delta^{13}C_{ini}$ represent the carbon isotopic compositions of DIC (‰) in the final state and initial component, respectively.

The calculation was constrained by the aqueous $\delta^{13}C$ (DIC) and gas $\delta^{13}C$ (CO_2), as well as the corresponding temperatures. The estimated equilibration temperature at depth in the geothermal system is ~166°C (Hahm et al., 2008). The observed temperatures of hot springs are 60–77°C, and the temperatures of rivers are ~10°C. The gas $\delta^{13}C$ ranges from −7.2‰ to −3.5‰ (Hahm et al., 2008), and the aqueous $\delta^{13}C$ is from −2.2‰ to 3.0‰ in the hot springs, whereas the highest $\delta^{13}C_{DIC}$ is 3.5‰ for the rivers (Table 1).

In this study, we considered the CO_2 outgassing in two stages (i.e., experiencing two different processes in Figures 6a and 6b). The first stage is outgassing from the groundwater during its ascent to the surface, and the second stage is outgassing at the Earth's surface (i.e., from hot springs and rivers; Figures 6a and 6b). At the circum-neutral pH of the springs and rivers, HCO_3^- is the dominant form of DIC. As the fractionation factor of $CO_{2(g)}$–$HCO_3^-{}_{(aq)}$ decreases with increasing temperature, for a given $\delta^{13}C_{DIC}$ value, it requires greater CO_2 loss at a higher temperature (M. J. Evans et al., 2008). In reality, the CO_2 outgassing takes place over a range of temperatures, and we calculated the limiting constraints of deep CO_2 outgassing fluxes. The model assumes the following constraints: (a) all the initial DIC in hot springs are assumed to have similar isotopic compositions, and the $\delta^{13}C_{ini}$ is the lowest measured gas $\delta^{13}C$ (i.e., −7.2‰) in the studied area; (b) CO_2 outgassing during the first stage takes place at the lowest temperature in hot springs (i.e., 60°C), and the $\delta^{13}C_{fin}$ for the first stage is the lowest $\delta^{13}C_{DIC}$ in hot springs; (c) CO_2 outgassing during the second stage takes place at the water temperature of rivers, and the $\delta^{13}C_{fin}$ for the second stage is the highest $\delta^{13}C_{DIC}$ in rivers (i.e., 3.5‰), neglecting the effects of surface water mixing (Figure 6b).

With the above conservative assumptions, we obtained the minimum degassing values (fraction of CO_2 lost) of 0.65 and 0.41 for the first and second stages, respectively (Figure 6b). So, in total, the minimum fraction degassing fraction (i.e., $1 - f_{DIC}$) was 0.79 (since the first step degassing is 0.65, and the second step degassing is 0.35×0.41) (Figure 6b). Based on the calculated degassing faction and remaining fraction, we estimate that the CO_2 outgassing flux is 1.24×10^4 t C yr^{-1} in the studied area. This is an underestimate of the deep CO_2 outgassing flux, since our assumptions are designed to minimize it.

4.3. The Net Carbon Budget Concerning Deep Carbon Release and Silicate Weathering

For each studied river basin, we combine the calculation of DIC_{Hyd} flux with deep CO_2 outgassing flux to estimate the total deep carbon release (1.57×10^4 t C yr^{-1}; 3.75 t C yr^{-1} km^{-2}) to the Earth's surface from the Changbaishan volcanic field. The total deep carbon release flux in the Changbaishan volcanic field only occupies a small proportion in global volcanic CO_2 release (70–100 MtC yr^{-1}; Hilton & West, 2020), but it has great impact on regional carbon cycle. Soil CO_2 in this study area was mainly from biogenic carbon (Sun et al., 2020), and soil respiration and plant photosynthesis do not affect the carbon cycling at geological timescales (Clark & Fritz, 1997; Hilton & West, 2020). We only investigate the processes affecting carbon cycling on geological timescales in this study, and therefore do not consider these modern processes. Combined with soil CO_2 consumed by silicate weathering (1.51×10^4 t C yr^{-1}; 3.60 t C yr^{-1} km^{-2}) and deep carbon released to the Earth's surface, we calculate that the net carbon budget is carbon source to the atmosphere of 0.06×10^4 t C yr^{-1} (0.14 t C yr^{-1} km^{-2}) for the studied area (Figure 7).

The total deep carbon release we obtain is an underestimate, so we are certain that the net CO_2 flux from the Changbaishan volcanic field is positive. In addition, our study focuses on the Changbaishan volcanic area within Chinese territory, and the Changbaishan volcanic area in North Korea has not been investigated. Thus, researches in wide study areas should be conducted to understand the carbon yields. This study verified that carbon budgets

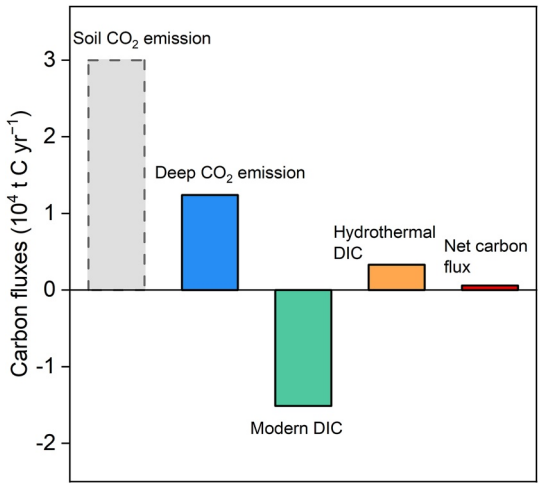

Figure 7. Net carbon balance due to CO_2 emission from hot springs, dissolved inorganic carbon (DIC) of biogenic and hydrothermal sources. The positive values represent a carbon source to the atmosphere, while the negative value represent carbon sink.

are complicated by adding deep carbon, and that $\Delta^{14}C_{DIC}$ can act as a probe in constraining the carbon sources in active volcanic area. Most previous studies on chemical weathering fluxes overlooked the contribution of deep carbon, and thus overestimated the role of silicate weathering on CO_2 consumption (cf. Dessert et al., 2003). Moreover, most previous studies on volcanic areas estimated the deep carbon release using $\delta^{13}C_{DIC}$, which overestimated the deep carbon contribution. Our results assessed the deep carbon fluxes using both $\Delta^{14}C_{DIC}$ and $\delta^{13}C_{DIC}$, which have great implications on understanding the role of chemical weathering and deep carbon release on atmospheric CO_2 in active volcanic areas.

5. Conclusions

Based on the chemical and isotopic compositions (i.e., major ion concentrations, $\delta^{13}C_{DIC}$ and $\Delta^{14}C_{DIC}$) in rivers, cold springs, hot springs, and crack rivers from Changbaishan volcanic area, Northeast China, we arrived to these conclusions:

1. The concentrations of most major ions were highly affected by mixing of solutes from hydrothermal fluids and those from low-temperature weathering, whereas low-temperature weathering mainly includes weathering of basalt and trachyte.
2. The hydrothermal DIC flux (i.e., deep carbon release in dissolved state) is 0.33×10^4 t C yr^{-1}, whereas the biogenic DIC flux is 1.51×10^4 t C yr^{-1} for the studied area, corresponding to a yield of 0.79 and 3.60 t C yr^{-1} km^{-2}, respectively.
3. The minimum deep CO_2 outgassing (i.e., deep carbon release in gaseous state) flux is 1.24×10^4 t C yr^{-1} based on isotopic fractionation of DIC and measured $\delta^{13}C_{DIC}$, and the total flux of deep carbon release is 1.57×10^4 t C yr^{-1}.
4. In the Changbaishan volcanic area, the net deep carbon flux (i.e., the sum of deep carbon release and chemical weathering consumption) to the atmosphere was 0.06×10^4 t C yr^{-1}, close to neutral but this net value is positive because the CO_2 outgassing flux is an underestimate.

Data Availability Statement

The data analyzed in this study can be found in Table 1 and are available online (at https://doi.org/10.5061/dryad.sj3tx968n).

Acknowledgments
This work was financially supported by the National Natural Science Foundation of China (Grants 41930642, 42173013, and 41925002). Antonio Caracausi appreciates support from the "Ramón y Cajal" research program (RYC2021-033270-I; MCIN/AEI/10.13039/501100011033-EU "NextGenerationEU/PRTR"). The authors acknowledge Yuanbi Yi and Shuai Chen for their help in sample analyses, and Sen Xu is acknowledged for his help in plotting.

References

Alling, V., Porcelli, D., Mörth, C. M., Anderson, L. G., Sanchez-Garcia, L., Gustafsson, Ö., et al. (2012). Degradation of terrestrial organic carbon, primary production and out-gassing of CO_2 in the Laptev and East Siberian Seas as inferred from $\delta^{13}C$ values of DIC. *Geochimica et Cosmochimica Acta*, *95*, 143–159. https://doi.org/10.1016/j.gca.2012.07.028

Andreeva, O. A., Yarmolyuk, V. V., Andreeva, I. A., Ji, J. Q., & Li, W. R. (2014). The composition and sources of magmas of Changbaishan Tianchi volcano (China-North Korea). *Doklady Earth Sciences*, *456*(1), 572–578. https://doi.org/10.1134/s1028334x14050213

Bai, X., Chetelat, B., & Song, Y. (2017). Sources of dissolved inorganic carbon in rivers from the Changbaishan area, an active volcanic zone in North Eastern China. *Acta Geochimica*, *36*(3), 410–415. https://doi.org/10.1007/s11631-017-0178-y

Barbieri, M., Boschetti, T., Barberio, M. D., Billi, A., Franchini, S., Iacumin, P., et al. (2020). Tracing deep fluid source contribution to groundwater in an active seismic area (central Italy): A combined geothermometric and isotopic ($\delta^{13}C$) perspective. *Journal of Hydrology*, *582*, 124495. https://doi.org/10.1016/j.jhydrol.2019.124495

Becker, J. A., Bickle, M. J., Galy, A., & Holland, T. J. B. (2008). Himalayan metamorphic CO_2 fluxes: Quantitative constraints from hydrothermal springs. *Earth and Planetary Science Letters*, *265*(3–4), 616–629. https://doi.org/10.1016/j.epsl.2007.10.046

Berner, R. A., & Caldeira, K. (1997). The need for mass balance and feedback in the geochemical carbon cycle. *Geology*, *25*(10), 955–956. https://doi.org/10.1130/0091-7613(1997)025<0955:TNFMBA>2.3.CO;2

Caracausi, A., Paternoster, M., & Nuccio, P. M. (2015). Mantle CO_2 degassing at Mt. Vulture volcano (Italy): Relationship between CO_2 outgassing of volcanoes and the time of their last eruption. *Earth and Planetary Science Letters*, *411*, 268–280. https://doi.org/10.1016/j.epsl.2014.11.049

Caudron, C., Mazot, A., & Bernard, A. (2012). Carbon dioxide dynamics in Kelud volcanic lake. *Journal of Geophysical Research: Solid Earth*, *117*(B5), B05102. https://doi.org/10.1029/2011jb008806

Chiodini, G., Caliro, S., Cardellini, C., Frondini, F., Inguaggiato, S., & Matteucci, F. (2011). Geochemical evidence for and characterization of CO_2 rich gas sources in the epicentral area of the Abruzzo 2009 earthquakes. *Earth and Planetary Science Letters*, *304*(3–4), 389–398. https://doi.org/10.1016/j.epsl.2011.02.016

Chiodini, G., Cardellini, C., Amato, A., Boschi, E., Caliro, S., Frondini, F., & Ventura, G. (2004). Carbon dioxide Earth degassing and seismogenesis in central and southern Italy. *Geophysical Research Letters*, *31*(7), L07615. https://doi.org/10.1029/2004gl019480

Chiodini, G., Cardellini, C., Di Luccio, F., Selva, J., Frondini, F., Caliro, S., et al. (2020). Correlation between tectonic CO_2 Earth degassing and seismicity is revealed by a 10-year record in the Apennines, Italy. *Science Advances*, *6*(35), eabc2938. https://doi.org/10.1126/sciadv.abc2938

Clark, I. D., & Fritz, P. (1997). *Environmental isotopes in hydrogeology*. Lewis Publishers.

Dessert, C., Dupré, B., Gaillardet, J., François, L. M., & Allègre, C. J. (2003). Basalt weathering laws and the impact of basalt weathering on the global carbon cycle. *Chemical Geology*, *202*(3–4), 257–273. https://doi.org/10.1016/j.chemgeo.2002.10.001

Dessert, C., Gaillardet, J., Dupre, B., Schott, J., & Pokrovsky, O. S. (2009). Fluxes of high- versus low-temperature water–rock interactions in aerial volcanic areas: Example from the Kamchatka Peninsula, Russia. *Geochimica et Cosmochimica Acta*, *73*(1), 148–169. https://doi.org/10.1016/j.gca.2008.09.012

Dong, K., Lang, Y., Hu, N., Zhong, J., Xu, S., Hauser, T.-M., & Gan, R. (2018). The new AMS facility at Tianjin University. *Radiation Detection Technology and Methods*, *2*(1), 30. https://doi.org/10.1007/s41605-018-0064-0

Evans, M. J., Derry, L. A., & France-Lanord, C. (2008). Degassing of metamorphic carbon dioxide from the Nepal Himalaya. *Geochemistry, Geophysics, Geosystems*, *9*(4), Q04021. https://doi.org/10.1029/2007gc001796

Evans, W. C., Bergfeld, D., McGimsey, R. G., & Hunt, A. G. (2009). Diffuse gas emissions at the Ukinrek Maars, Alaska: Implications for magmatic degassing and volcanic monitoring. *Applied Geochemistry*, *24*(4), 527–535. https://doi.org/10.1016/j.apgeochem.2008.12.007

Evans, W. C., van Soest, M. C., Mariner, R. H., Hurwitz, S., Ingebritsen, S. E., Wicks, C. W., & Schmidt, M. E. (2004). Magmatic intrusion west of Three Sisters, central Oregon, USA: The perspective from spring geochemistry. *Geology*, *32*(1), 69–72. https://doi.org/10.1130/g19974.1

Gaillardet, J., Dupré, B., Louvat, P., & Allègre, C. J. (1999). Global silicate weathering and CO_2 consumption rates deduced from the chemistry of large rivers. *Chemical Geology*, *159*(1–4), 3–30. https://doi.org/10.1016/s0009-2541(99)00031-5

Gaillardet, J., & Galy, A. (2008). Atmospheric science. Himalaya—carbon sink or source? *Science*, *320*(5884), 1727–1728. https://doi.org/10.1126/science.1159279

Genereux, D. P., Webb, M., & Solomon, D. K. (2009). Chemical and isotopic signature of old groundwater and magmatic solutes in a Costa Rican rain forest: Evidence from carbon, helium, and chlorine. *Water Resources Research*, *45*(8), W08413. https://doi.org/10.1029/2008wr007630

Hahm, D., Hilton, D. R., Cho, M., Wei, H., & Kim, K. R. (2008). Geothermal He and CO_2 variations at Changbaishan intra-plate volcano (NE China) and the nature of the sub-continental lithospheric mantle. *Geophysical Research Letters*, *35*(22), L22304. https://doi.org/10.1029/2008gl035955

Hilton, R. G., & West, A. J. (2020). Mountains, erosion and the carbon cycle. *Nature Reviews Earth & Environment*, *1*(6), 284–299. https://doi.org/10.1038/s43017-020-0058-6

James, E. R., Manga, M., & Rose, T. P. (1999). CO_2 degassing in the Oregon Cascades. *Geology*, *27*(9), 823–826. https://doi.org/10.1130/0091-7613(1999)027<0823:Cditoc>2.3.Co;2

Keeling, C. D. (1958). The concentration and isotopic abundances of atmospheric carbon dioxide in rural areas. *Geochimica et Cosmochimica Acta*, *13*(4), 322–334. https://doi.org/10.1016/0016-7037(58)90033-4

Kis, B.-M., Ionescu, A., Cardellini, C., Harangi, S., Baciu, C., Caracausi, A., & Viveiros, F. (2017). Quantification of carbon dioxide emissions of Ciomadul, the youngest volcano of the Carpathian-Pannonian Region (Eastern-Central Europe, Romania). *Journal of Volcanology and Geothermal Research*, *341*, 119–130. https://doi.org/10.1016/j.jvolgeores.2017.05.025

Lai, Q. (2019). *Research on ecological base flow and mineral water in basalt area of Changbai Mountain*. Jilin University. (in Chinese with English abstract).

Lewicki, J. L., Hilley, G. E., Dobeck, L., McLing, T. L., Kennedy, B. M., Bill, M., & Marino, B. D. V. (2013). Geologic CO_2 input into groundwater and the atmosphere, Soda Springs, ID, USA. *Chemical Geology*, *339*, 61–70. https://doi.org/10.1016/j.chemgeo.2012.06.013

Li, G., Hartmann, J., Derry, L. A., West, A. J., You, C. F., Long, X., et al. (2016). Temperature dependence of basalt weathering. *Earth and Planetary Science Letters*, *443*, 59–69. https://doi.org/10.1016/j.epsl.2016.03.015

Lin, L. (2016). *The research on the genesis and the exploitation control scheme of the mineral spring water resource in the Changbai Mountain District*. Jilin University. (in Chinese with English abstract).

Mao, X., Wang, H., & Feng, L. (2018). Impact of additional dead carbon on the circulation estimation of thermal springs exposed from deep-seated faults in the Dongguan basin, southern China. *Journal of Volcanology and Geothermal Research*, *361*, 1–11. https://doi.org/10.1016/j.jvolgeores.2018.08.002

Marwick, T. R., Tamooh, F., Teodoru, C. R., Borges, A. V., Darchambeau, F., & Bouillon, S. (2015). The age of river-transported carbon: A global perspective. *Global Biogeochemical Cycles*, *29*(2), 122–137. https://doi.org/10.1002/2014gb004911

Mayorga, E., Aufdenkampe, A. K., Masiello, C. A., Krusche, A. V., Hedges, J. I., Quay, P. D., et al. (2005). Young organic matter as a source of carbon dioxide outgassing from Amazonian rivers. *Nature*, *436*(7050), 538–541. https://doi.org/10.1038/nature03880

Menzies, C. D., Wright, S. L., Craw, D., James, R. H., Alt, J. C., Cox, S. C., et al. (2018). Carbon dioxide generation and drawdown during active orogenesis of siliciclastic rocks in the Southern Alps, New Zealand. *Earth and Planetary Science Letters*, *481*, 305–315. https://doi.org/10.1016/j.epsl.2017.10.010

Mook, W. G., Bommerson, J. C., & Staverman, W. H. (1974). Carbon isotope fractionation between dissolved bicarbonate and gaseous carbon dioxide. *Earth and Planetary Science Letters*, *22*(2), 169–176. https://doi.org/10.1016/0012-821x(74)90078-8

Niu, Z., Zhou, W., Cheng, P., Wu, S., Lu, X., Xiong, X., et al. (2016). Observations of atmospheric $\Delta^{14}CO_2$ at the global and regional background sites in China: Implication for fossil fuel CO_2 inputs. *Environmental Science & Technology*, *50*(22), 12122–12128. https://doi.org/10.1021/acs.est.6b02814

Perez, N. M., Hernandez, P. A., Padilla, G., Nolasco, D., Barrancos, J., Melian, G., et al. (2011). Global CO_2 emission from volcanic lakes. *Geology*, *39*(3), 235–238. https://doi.org/10.1130/g31586.1

Polsenaere, P., & Abril, G. (2012). Modelling CO_2 degassing from small acidic rivers using water pCO_2, DIC and δ^{13}C-DIC data. *Geochimica et Cosmochimica Acta*, *91*, 220–239. https://doi.org/10.1016/j.gca.2012.05.030

Rivé, K., Gaillardet, J., Agrinier, P., & Rad, S. (2013). Carbon isotopes in the rivers from the Lesser Antilles: Origin of the carbonic acid consumed by weathering reactions in the Lesser Antilles. *Earth Surface Processes and Landforms*, *38*(9), 1020–1035. https://doi.org/10.1002/esp.3385

Seward, T. M., & Kerrick, D. M. (1996). Hydrothermal CO_2 emission from the Taupo Volcanic Zone, New Zealand. *Earth and Planetary Science Letters*, *139*(1–2), 105–113. https://doi.org/10.1016/0012-821x(96)00011-8

Shangguan, Z., Zheng, Y., & Dong, J. (1997). Material sources of escaped gases from Tianchi volcanic geothermal area, Changbai Mountains. *Science in China - Series D: Earth Sciences*, *40*(4), 390–397. https://doi.org/10.1007/bf02877570

Stefánsson, A., Sveinbjörnsdóttir, Á. E., Heinemeier, J., Arnórsson, S., Kjartansdóttir, R., & Kristmannsdóttir, H. (2016). Mantle CO_2 degassing through the Icelandic crust: Evidence from carbon isotopes in groundwater. *Geochimica et Cosmochimica Acta*, *191*, 300–319. https://doi.org/10.1016/j.gca.2016.06.038

Sun, Y., Guo, Z., & Fortin, D. (2020). Carbon dioxide emission from monogenetic volcanoes in the Mt. Changbai volcanic field, NE China. *International Geology Review*, *63*(14), 1803–1820. https://doi.org/10.1080/00206814.2020.1802782

Svensen, H., & Jamtveit, B. (2010). Metamorphic fluids and global environmental changes. *Elements*, *6*(3), 179–182. https://doi.org/10.2113/gselements.6.3.179

Wei, H., Liu, G., & Gill, J. (2013). Review of eruptive activity at Tianchi volcano, Changbaishan, Northeast China: Implications for possible future eruptions. *Bulletin of Volcanology*, *75*(4), 706. https://doi.org/10.1007/s00445-013-0706-5

Xu, X., Trumbore, S. E., Zheng, S., Southon, J. R., McDuffee, K. E., Luttgen, M., & Liu, J. C. (2007). Modifying a sealed tube zinc reduction method for preparation of AMS graphite targets: Reducing background and attaining high precision. *Nuclear Instruments and Methods in Physics Research Section B: Beam Interactions with Materials and Atoms*, *259*(1), 320–329. https://doi.org/10.1016/j.nimb.2007.01.175

Yan, B., Qiu, S., Liu, Z., & Changlai, X. (2017). Characteristics of the geothermal water in Changbai Mountain volcanic region, northeast of China. *Arabian Journal of Geosciences*, *10*(12), 261. https://doi.org/10.1007/s12517-017-3039-4

Zhang, M., Guo, Z., Sano, Y., Cheng, Z., & Zhang, L. (2015). Stagnant subducted Pacific slab-derived CO_2 emissions: Insights into magma degassing at Changbaishan volcano, NE China. *Journal of Asian Earth Sciences*, *106*, 49–63. https://doi.org/10.1016/j.jseaes.2015.01.029

Zhong, J., Li, S.-L., Liu, J., Ding, H., Sun, X., Xu, S., et al. (2018). Climate variability controls on CO_2 consumption fluxes and carbon dynamics for monsoonal rivers: Evidence from Xijiang River, Southwest China. *Journal of Geophysical Research: Biogeosciences*, *123*(8), 2553–2567. https://doi.org/10.1029/2018jg004439

Zhong, J., Li, S., Li, Z., Zhu, X., Yi, Y., Ma, T., et al. (2022). Metamorphic fluxes of water and carbon in rivers of the eastern Qinghai-Tibetan Plateau. *Science China Earth Sciences*, *65*(4), 652–661. https://doi.org/10.1007/s11430-021-9873-7

Zhong, J., Wallin, M. B., Wang, W., Li, S. L., Guo, L., Dong, K., et al. (2021). Synchronous evaporation and aquatic primary production in tropical river networks. *Water Research*, *200*, 117272. https://doi.org/10.1016/j.watres.2021.117272

Zhu, Y., She, Z., Fu, D., Huang, X., Li, X., & Mao, X. (1981). The hydrochemistry of Tianchi (Crater) lake of the Changbai Mountains. *Scientia Geographica Sinica*, *1*(1), 58–65. https://doi.org/10.13249/j.cnki.sgs.1981.01.007